

The Oxidation Mechanism of Pure Aluminum Powder Particles

S. Hasani · M. Panjepour · M. Shamanian

Received: 23 December 2011 / Revised: 15 March 2012 / Published online: 22 May 2012
© Springer Science+Business Media, LLC 2012

Abstract The oxidation mechanism of aluminum powder particles was studied by simultaneous TG–DTA analysis (under air atmosphere) at different heating rates (10, 20 and 30 °C/min) and from an ambient temperature up to 1,400 °C. Also, the rate of oxidation reaction (rate of weight gain; RTG) was obtained by the differentiation of weight gain (TGG) curve. Additionally, SEM and X-ray diffraction analysis (XRD) studies were performed on each of the above samples for their structural and phase studies. The results obtained from TG–DTA and RTG curves; microstructure and phase analysis studies indicated that the oxidation of aluminum powders occurred during five stages. On the other hand, according to the results obtained from XRD and TGG curves, aluminum particles after the thermal analysis test, even heated up to 1,400 °C, were not entirely oxidized (i.e. less than 10 %).

Keywords Aluminum powder · Oxidation · Mechanism · Non-isothermal reaction · Heating rate · Alumina

Introduction

Within the recent few decades, aluminum powders have been widely used for aluminothermic processes, propellants, launch cost, fireworks, and explosives [1–7]. In fact, oxidation enthalpy, high combustion heat, low cost, and production of safe products for ecosystem are of the specifications of the oxidation process of aluminum powders [8]. For this reason, researchers have paid attention to the study

S. Hasani · M. Panjepour (✉) · M. Shamanian
Department of Materials Engineering, Isfahan University of Technology, 84156-83111 Isfahan, Iran
e-mail: panjepour@cc.iut.ac.ir

S. Hasani
e-mail: s.hasani@ma.iut.ac.ir

of the mechanism of oxidation process in recent years and some studies have been performed on this process and the combustion temperature of aluminum.

The combustion temperature for aluminum powders was reported to be from 650 to 2,000 °C during 1968–1997 by researchers [9–13]. Also, the combustion temperature for the aluminum nano-powders was reported to be about 800 °C and even less than that by Johnson et al. [14] in 2000. In fact, the discrepancy among the obtained results shows the great complexity of this process. However, after the protective role of the thin aluminum oxide film on the surface of aluminum particles was cleared up, it was first believed that the oxidation of these particles must have taken place around the melting point of Al_2O_3 (2,054 °C), i.e. when the continuous uniformity of the surface crust was destroyed (because of melting or mechanical tensions) [15, 16]. The studies performed in 2000 and 2002 specified that a thin layer of aluminum oxide in amorphous form (non-stoichiometric Al_2O_3) was formed on the surface of aluminum. At low thickness, this amorphous oxide film consists of enriched aluminum and is thermodynamically more stable than the crystalline state unless it reaches a critical thickness [17–19]. It is worth mentioning that the growth of this amorphous oxide layer is controlled by the diffusion of aluminum cations to the outer part [20], so that the presence of more aluminum in the structure prevents it from crystallization. On heating the Al- μm particles begin to form a $\gamma\text{-Al}_2\text{O}_3$ scale before reaching the melting point and the molten Al is kept within the $\gamma\text{-Al}_2\text{O}_3$ shell [21]. In fact, by an increase in temperature ($T > 300$ °C), the thickness of the amorphous oxide layer reaches a critical point and at this point it is changed into alumina with $\gamma\text{-Al}_2\text{O}_3$ crystalline structure [19]. The critical thickness for this amorphous oxide layer is reported to be from 0.5 nm [20] to 4 nm [22] in different references. Additionally, by the formation of crystalline structure of $\gamma\text{-Al}_2\text{O}_3$ phase and appearance of grain boundary, the rate of oxidation is increased as a result of the ease of oxygen diffusion through the grain boundary [23]. On the other hand, the studies performed by Mikhaylo et al. [24] specified that the crystallization of the oxide layer was related to $\gamma\text{-Al}_2\text{O}_3$ phase which has a higher density than the amorphous state. So, during this course of phase transformation, formation of micro-cracks on the oxide crust is not surprising. Hence, the presence of grain boundaries and probably the presence of the produced micro-cracks have facilitated the diffusion trend for the preparation of the oxidation at this stage. After this stage builds a layer of 6–10 nm thickness composed of crystallites of the same size independent on the initial particle size [25]. The same of results [20, 22] shown that at this stage, oxygen diffusion is the controlling factor for the process and growth rate of $\gamma\text{-Al}_2\text{O}_3$, while Eisenreich et al. [25] shown that this reaction is dominated by chemical kinetics and converts a substantial fraction of the particle. The reasons of this difference can be because Influence of the metal particle size [25, 26]. By continuing the oxidation, the micro-cracks present (i.e. the quick penetration paths) in the oxide layer are repaired and a layer of $\gamma\text{-Al}_2\text{O}_3$ oxide covers the surface of the aluminum powder particles. At this time, the rate of oxidation is once more reduced.

On further heating $\theta\text{-Al}_2\text{O}_3$ can be detected, which forms simultaneously with the $\gamma\text{-Al}_2\text{O}_3$. The $\gamma\text{-Al}_2\text{O}_3/\theta\text{-Al}_2\text{O}_3$ scale is stable and protective under isothermal conditions up to 800 °C within the investigated times [24]. On further heating the $\gamma\text{-Al}_2\text{O}_3$ and $\theta\text{-Al}_2\text{O}_3$, transform simultaneously to $\alpha\text{-Al}_2\text{O}_3$ in a temperature range

of 850–1,100 °C [24]. The α -Al₂O₃ phase can be generated directly from the γ -Al₂O₃ phase or indirectly from the middle phases of θ and δ . The densities of γ , θ and δ phases are not so different from each other. Therefore, the phase changes among the above phases will not bring about any changes in the oxidation process [23]. During the γ transformation to α -Al₂O₃ shrinkage occurs that leads to formation of pores [24]. Finally, by the start of ignition temperature and with regard to the size of the particles, intense oxidation takes place in the particles [23].

In spite of the extensive researches performed in this area, the role of aluminum melt and its manner of affecting the trend of oxidation have not been taken into consideration yet. Additionally, there is no good conformity between the proposed mechanisms for this process and laboratory results, especially the microscopic examinations. This lack of conformity signifies the necessity for more study to be done on this process. For this reason, in this investigation it has been tried to study the mechanism of the oxidation of aluminum particles more precisely by taking advantage from the studies performed by TG–DTA thermal analysis, scanning electron microscope (SEM), and X-ray diffraction analysis (XRD).

Materials and Methodology

The 99 % pure aluminum powder (Fluka Company) with a grain size of 100–200 μm was used in this study. To study the mechanism of aluminum oxidation, the experiments were carried out in a STA device (STA503, Bahr) capable of simultaneous TG–DTA analysis within the temperature ranges from 25 to 720, 900 and 1,400 °C. The aluminum powder samples were oxidized directly (as non-isothermally and under air atmosphere) in the STA device. Different parameters of these tests are presented in Table 1. In addition to that, in order to gain more accurate information on the changes taking place within the specified temperature, some consumable aluminum powders were isothermally heat treated. For this purpose, the consumable aluminum powders were heat treated (under air atmosphere) at 900 °C for 15 min. In the next stage, the microstructure of the products was analyzed by SEM (XL30 SERIES, Philips) and the phase analysis was performed by XRD (MPD-XPRT, Philips), respectively.

Table 1 The sample weight and the specifications of TG–DTA experiments

No.	W_0 : the initial weight of sample (mg)	T_{max} (°C)	Heating rate (°C/min)
1	35.92	1,400	10
2	35.02	1,400	20
3	35.27	1,400	30
4	35.36	720	20
5	35.06	900	20

Results and Discussion

Thermal Analysis

The typical TG–DTA curves of the sample (at a heating rate of 20 °C/min) are shown in Fig. 1. This figure is presented to better understand and gain enough recognition of the phenomena performed on the basis of these curves, including the characteristic temperatures of oxidation process (T_1 to T_7). Each TG–DTA curves can be divided into different regions (I to V). Hence, the results obtained from the thermal analysis experiments, consisting of TG–DTA and the characteristic points of the reaction curves, performed on the aluminum powders at the heating rates of 10, 20, and 30 °C/min (according to Table 1), are presented in Fig. 2a, b, c and Tables 2, 3. As it is observed in Fig. 2a, b, c, in TG–DTA curves no change takes place in the course of the stages of the oxidation process of aluminum powders at different heating rates. Tables 2 and 3 show the influence of heating rate on the characteristic temperatures and ΔW differences at the five regions of I to V. The definition of TGG (weight gain of the sample) and rate of weight gain (RTG) are as follows:

$$TGG (\%) = \frac{\Delta W_t}{\Delta W_{max}} \times 100 \tag{1}$$

$$RTG (\%/s) = \frac{d(TGG)}{dt} \times 100 = \frac{d(\Delta W_t / \Delta W_{max})}{dt} \times 100 \tag{2}$$

where, ΔW_t is the observed weight gain of the sample arbitrary time t (or temperature T) and ΔW_{max} is the theoretical weight gain of the sample after completion of

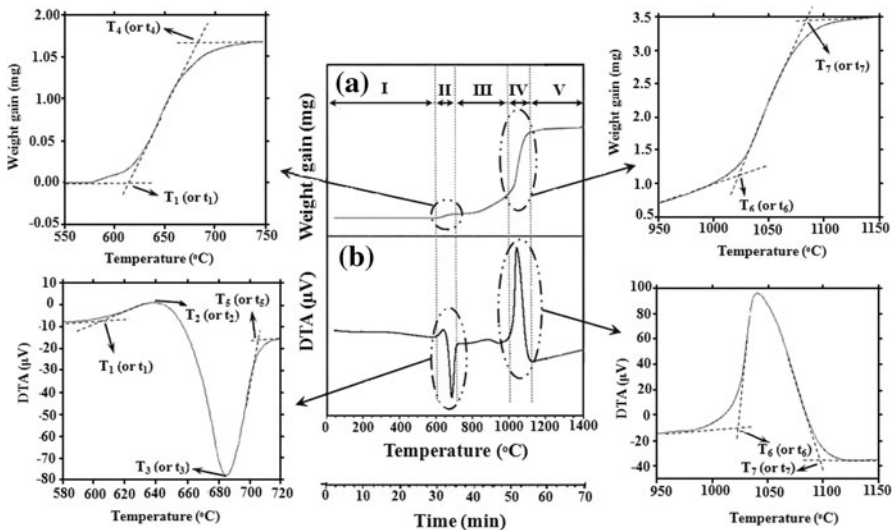


Fig. 1 Typical results of TG (weight gain)-DTA curves and definitions of characteristic regions and temperatures for the oxidation process of aluminum powders, with a constant heating rate of 20 °C/min

Table 2 The influence of heating rate on the characteristic temperatures and times (extracted from TG-DTA curves)

Heating rate (°C/min)	Observed of oxidation experiment (TG-DTA)													
	T _i (°C)							t _i (min)						
i = 1	i = 1	i = 2	i = 3	i = 4	i = 5	i = 6	i = 7	i = 1	i = 2	i = 3	i = 4	i = 5	i = 6	i = 7
10	590	616	676	680	683	990	1070	56.2	58.8	64.8	65.2	65.5	96.2	104.2
20	610	640	685	687	705	1025	1090	29.1	30.6	32.8	33.0	33.9	49.9	53.1
30	616	653	695	700	713	1030	1120	19.6	20.8	22.2	22.4	22.8	33.4	36.4

Table 3 The results extracted from TGG and RTG curves; theoretical and observed weight gain of samples at various heating rates

No.	Heating rate (°C/min)	Oxidation experiment (TG–DTA)										
		Theoretical		Observed							RTG _{max} (%/s)	
		W _{max} (mg)	ΔW _{max} (mg)	ΔW _t (mg)					(ΔW _t /ΔW _{max}) × 100 (%)	Region II	Region IV	
		t = t ₁	t = t ₄	t = t ₆	t = t ₇	t = t _f ^a						
1	10	67.87	31.95	0.10	0.18	0.70	1.80	1.95	6.10	0.25	2.20	
2	20	66.17	31.15	0.10	0.19	0.75	2.11	2.33	7.50	0.30	2.80	
3	30	66.64	31.37	0.12	0.38	0.88	2.76	3.07	9.78	0.40	3.00	

^a $t_f = t_{max}$ (or $T_f = T_{max} = 1,400$ °C)

the reaction. It means that the weight gain from the beginning of the experiment can be determined by the following equations, respectively:

$$\Delta W_t = W_t - W_0 \quad (3)$$

$$\Delta W_{max} = W_{max} - W_0 \quad (4)$$

where, W_t represents the weight of the sample at arbitrary time t (or temperature T), and W_{max} is the weight of sample after completion of the reaction.

As it is observed in the TG and RTG curves in Fig. 2a, b, c, there is no peak or any weight increase up to the temperature limit of 600 °C (Table 3). This is indicative of the fact that no significant oxidation has taken place within the temperature range of 25 °C to T_f (region I). With regard to the intense affinity of aluminum to oxidation even at low temperatures (e.g. room temperature), therefore the formation of an oxide crust on the particles of aluminum powder is certain. Subsequently, the DTA curves also support the results obtained from the TG and RTG curves within this region. In spite of this fact and observations, it can be concluded that the oxide crust performs its role of protecting aluminum within the temperature region I and thus no noticeable oxidation takes place at this stage. Additionally, the studies performed by Jeurgens et al. [20] also show that the structure of the oxide film is amorphous and because of the permeation of aluminum cations within region I, the process of oxidation is limited to the outer part of this crust.

According to TG and RTG curves (Fig. 2a, b, c; Table 3), as the temperature is increasing a sudden increase in weight (TGG %) is observed around T_1 (at the beginning of region II). Along with this TGG (%) increase, an exothermic peak is also observed in the DTA curves. These observations are indicative of the intensification of oxidation within this heat limit. The studies done by Levin et al. [27] show that the amorphous oxide film is changed into γ -Al₂O₃ phase within this heat limit; while the density of the amorphous oxide film and the γ -Al₂O₃ is reported to be 3.1 and 3.65 g/cm³, respectively. With regard to these results, it can be concluded that due to this phase change and in spite of the structural change of oxide film from amorphous to crystalline state and higher density of γ -Al₂O₃ phase

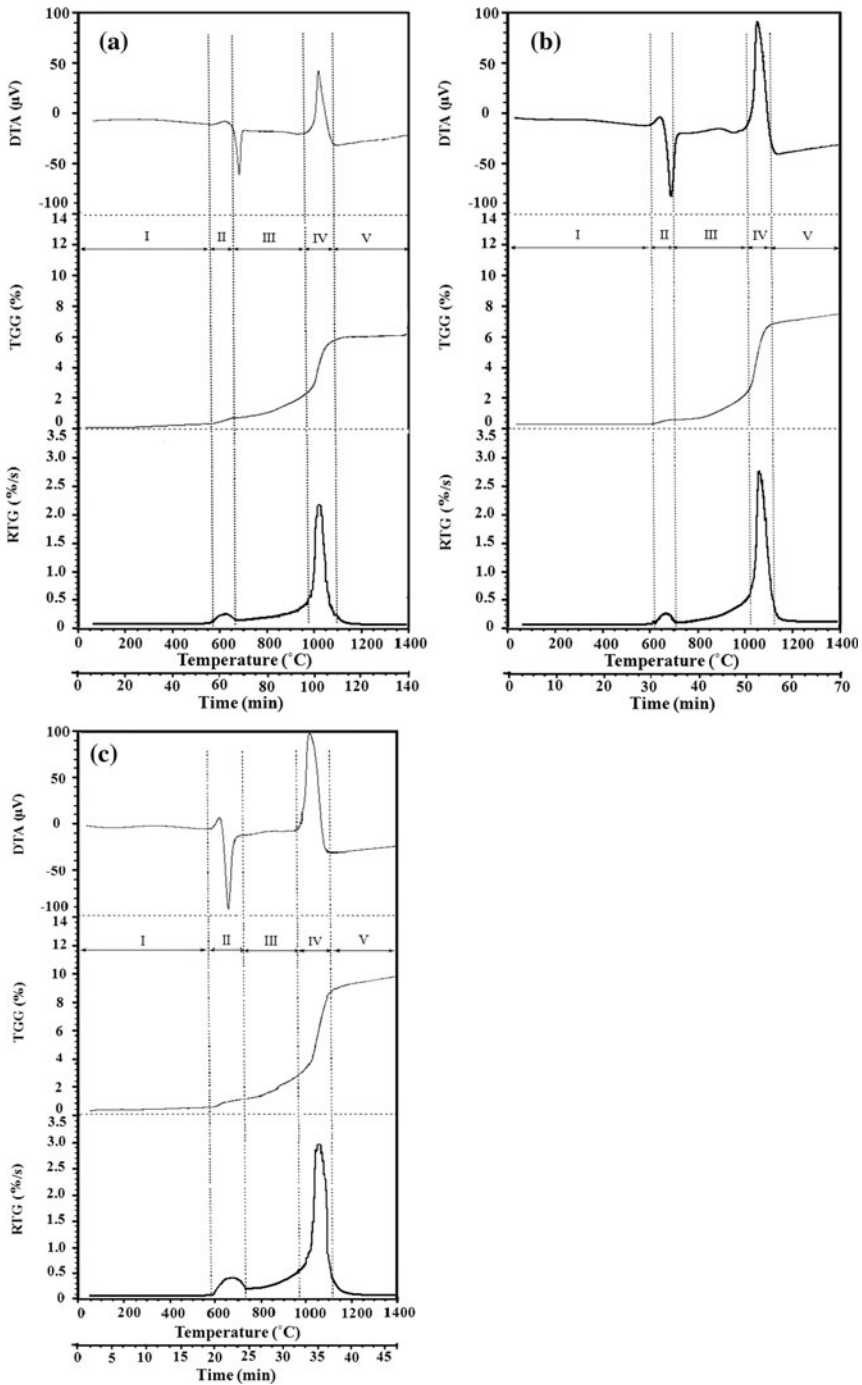


Fig. 2 TGG, DTA, and RTG curves for the oxidation process of aluminum powders at different heating rates; **a** 10 °C/min, **b** 20 °C/min, and **c** 30 °C/min

in relation to amorphous phase (about 20 vol%), there appears to be some micro-cracks in the crust. Generation of these micro-cracks means the loss of continuity of the oxide protective cover on the surface of aluminum particles. Besides that, because of the crystallization of the oxide layer, the grain boundary is generated in the form of a fast diffusion network in the crust structure. Hence, the presences of grain boundaries and probably micro-cracks have facilitated the diffusion trend for the preparation of the oxidation in region II. In other words, by increasing the temperature up to T_4 (at the end of region II), there is a continuous TGG (%) increase in the TG curve. While, in its corresponding DTA curve, the above exothermic peak is suddenly affected by the latent heat of aluminum melting at 660 °C. In fact, this phenomenon is indicative of the overlapping of two peaks of exothermic (resulting from oxidation process) and endothermic (resulting from the aluminum melt). As it is observed in this region, the intensity of the endothermic process of the aluminum melt has overshadowed the exothermic process of oxidation. For this reason, the DTA curves cannot depict this stage completely.

By an increase in temperature from T_4 to T_6 (region III), this increase in rate of oxidation reaction is reduced again, because the defects including the micro-cracks created on the surface are repaired during oxidation at this stage. So, the diffusion of oxygen to Al/Al₂O₃ interface will again face with difficulties. These changes in the rate of oxidation are well presented in the RTG curves in Fig. 2a, b, c. Therefore, in region III no noticeable TGG (%) (less than % 1.8) and heat flow (DTA μ V) are observed.

By continuing to increase the temperature from T_6 to T_7 (region IV), a noticeable increase in TGG (%) as well as in heat flow (in the form of exothermic peak) is obtained (Fig. 2a, b, c; Table 3). Also, as mentioned in “Introduction” section, by entering this region (the temperature from 1,000 to 1,100 °C), the γ -Al₂O₃ phase is transformed to α -Al₂O₃ phase [27]. However, the issue ignored by researchers is the situation of the aluminum turned into a melting state from 660 °C and remains

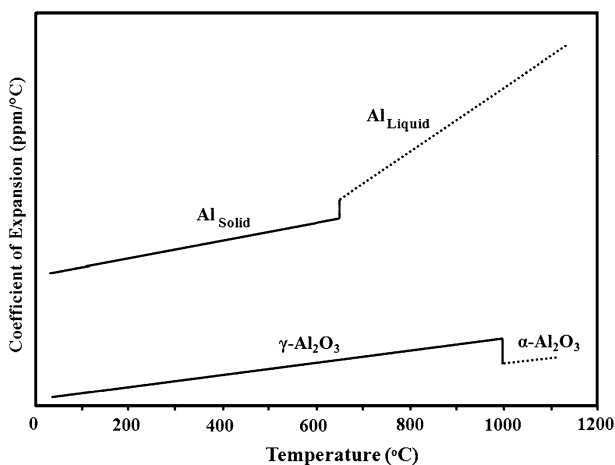


Fig. 3 The variation of thermal expansion coefficient for aluminum, γ -Al₂O₃ and α -Al₂O₃ versus temperature

imprisoned inside the oxide crust. As shown in Fig. 3 (adopted from Ref. [17]), by increasing the temperature, the melt starts expanding and by this change of volume, an added tension is exerted on the crust. Additionally, according to the result obtained by Jeurgens et al. [17], it can be reasoned that the aluminum thermal expansion coefficient is ten times larger than γ - Al_2O_3 . In addition, we know that the expansion in liquid phase is generally much more than in a solid phase. Consequently, according to Fig. 3, this melt expands more than the oxide crust (γ - Al_2O_3) when heat is increased. On the other hand, when γ - Al_2O_3 (cubic-fcc high disorder structure) transforms into α - Al_2O_3 (ordered structure with hexagonal close packed oxygen lattice and higher atomic density), volume shrinkage of 13.8 % occurs [21]. As shown in Fig. 4a, b, now if the tension resulting from shrinkage of crust and expansion of melting are so much that it can overcome the strength of the crust, so that pores and cracks [21] form in the crust scale during this transformation. In other word, forced by the oxide shell shrinkage and expansion of melting, molten aluminum can now penetrate outside through the pores and cracks and is immediately oxidized when getting in contact with air. For this reason, within region IV, intense exothermic peaks in the DTA curves and an intense TGG (%) increase in the TG curves are observed. In fact, the tension resulting from the oxide shell shrinkage and expansion of melting is able to tear the oxide crust within the temperature limit of 1,000 °C. This oxidation causes the liberation of a great amount of heat and a sudden and great amount of increase in weight. In other words, according to Table 3, the main stage of the oxidation of aluminum powder particles is done at this region. By the continuation of oxidation in the region, the cracks resulting from the tear of the oxide layer is repaired and the aluminum inside is protected against further oxidation. Hence, from T_7 to 1,400 °C (region V), no noticeable change is observed in any of the curves (Fig. 2a, b, c).

As observed in Fig. 2a, b, c and Table 3 (within regions II and IV), by increasing the heating rate, the intense peaks in the RTG curves also increase. This means that the rate of oxidation of aluminum powder particles is strongly dependent on the heating rate. Additionally, the maximum TGG (%) of the samples at different heating rates is only about 10 % (Table 3) up to 1,400 °C. Therefore, it can be concluded that the complete oxidation process did not take place even up to 1,400 °C.

Microstructure Observations

Figure 5 is related to the initial aluminum particles (before being exposed to oxide conditions). As it is observed in this figure, the surfaces of these particles enjoy high smoothness. In order to collect more precise information about the manner of the phase change and the phenomenon of the crystallization of the amorphous oxide layer in region II, the morphology of the product obtained from TG–DTA experiment at the maximum temperature of 720 °C using the heating rate of 20 °C/min, is shown by Fig. 6a, b. In this figure the change of amorphous oxide film to the crystalline γ - Al_2O_3 phase (as it was pointed out in the previous studies [27]) within this region is clearly depicted. In other words, the formation of γ - Al_2O_3 grains and grain boundaries during heating is well observed in the figure. Also, the size of the

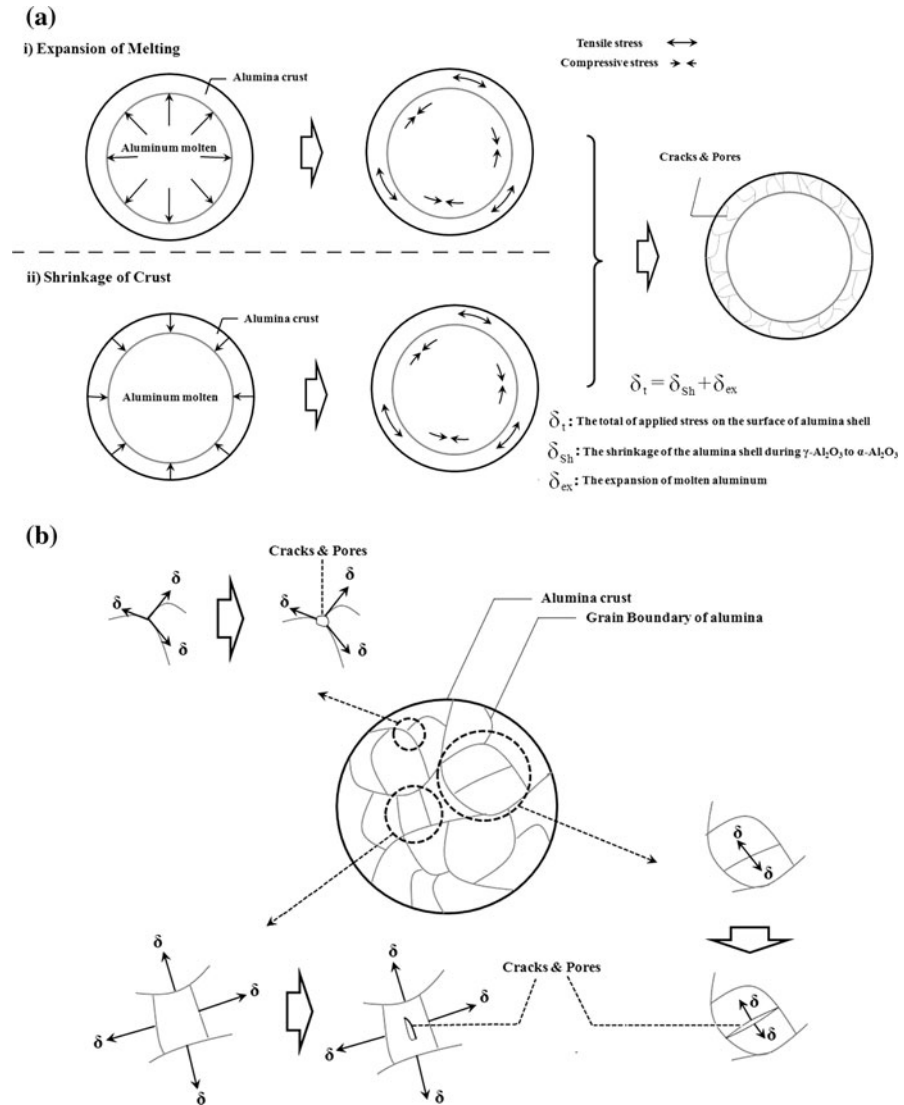


Fig. 4 a, b Schematic representation of cracks and pores formation

formed grains in this state is about 1–10 μm . Therefore, by comparing Figs. 5, and 6a, b, it can be concluded that due to the development of these grain boundaries and micro-cracks, the penetration paths in the oxide layer are increased which in turn brings about an increase in the rate of oxidation within region II. Figure 7 also shows the product obtained from TG–DTA experiment, using the heating rate of 20 $^{\circ}\text{C}/\text{min}$ at a maximum temperature of 900 $^{\circ}\text{C}$. But, as it is observed in Fig. 7, by increasing the temperature and by the continuation of the oxidation trend in region III, the grain boundaries and micro-cracks present in the oxide crust are repaired and

Fig. 5 SEM observation of the aluminum particles before experiment at the ambient temperature

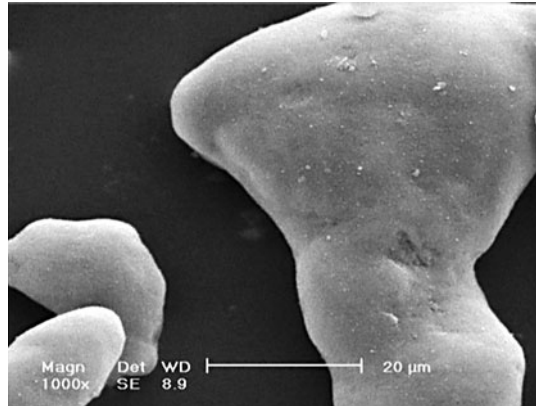
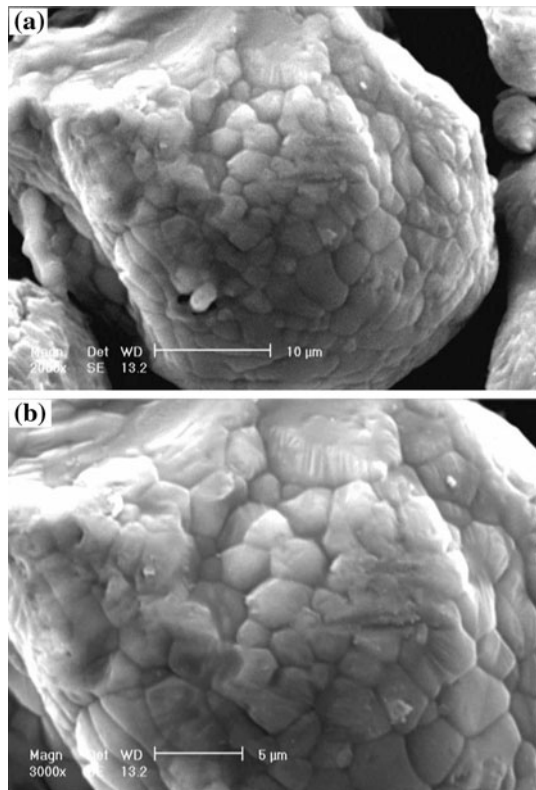


Fig. 6 SEM micrographs of an aluminum particle (by various magnifications) after being oxidized at the maximum temperature of 720 °C using the heating rate of 20 °C/min; surface structure at the various magnifications



changed again into a continuous oxide crust (according to Fig. 2a, b, c). On the other hand, as it was noted in “[Introduction](#)” section, due to the higher density of γ - Al_2O_3 phase relative to the amorphous oxide film [27], there is the possibility of crust cracking and development of micro-cracks during this transformation. Hence, in order to obtain more precise information about the manner of the micro-cracks

Fig. 7 SEM micrographs of the aluminum particles after being oxidized at the maximum temperature of 900 °C at the heating rate of 20 °C/min; surface structure (grain and grain boundaries)

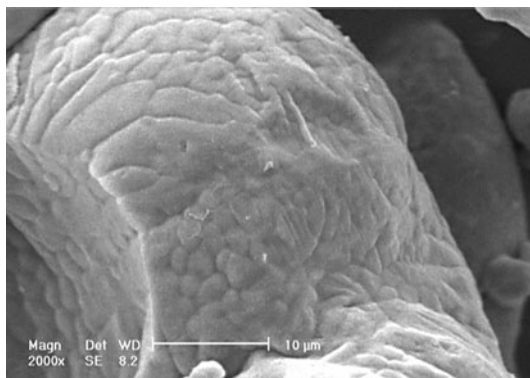
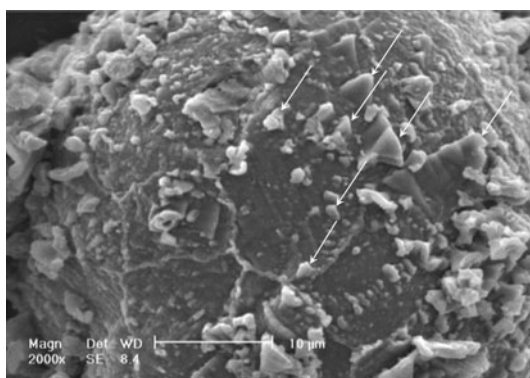


Fig. 8 SEM micrographs of aluminum particles after being oxidized at the maximum temperature of 1,400 °C by the heating rate of 20 °C/min; the needles and plate on the surface of particle aluminum

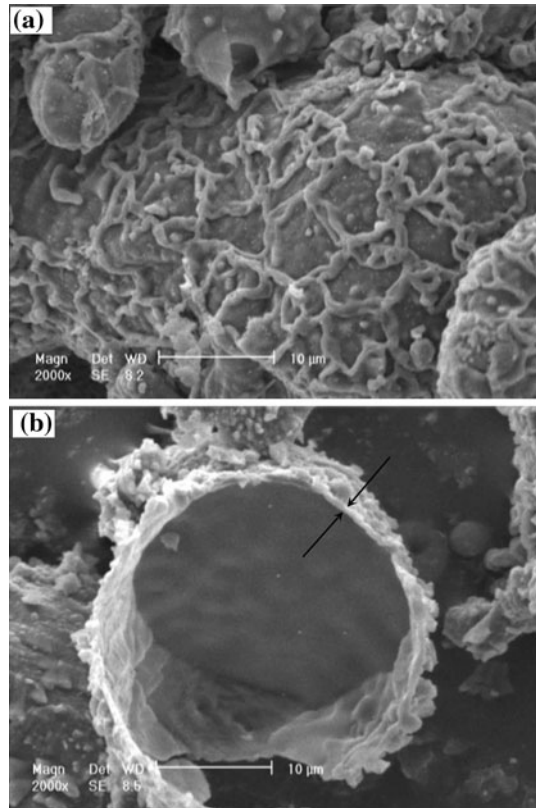


formation. It should be mentioned that after the change of the amorphous crust phase to the γ - Al_2O_3 crystalline structure, the aluminum in the crust melted. With regard to this point, if the theory of the formation of micro-cracks at higher temperature (i.e. region III) were true for reasons other than those mentioned, then they would be accompanied by the permeation of inner melt through the micro-cracks.

It was also mentioned that when the temperature reached about 660 °C, the melting of aluminum could not bring about a noticeable change in the trend of oxygen diffusion through the oxide crust. But this fact cannot be ignored that by increasing the temperature, the volume of the molten aluminum is also increased in a way that it exerts great tension on the oxide crust. Additionally in this stage, the shrinkage in the alumina scale during the γ - Al_2O_3 to α - Al_2O_3 transformation increase tension on the oxide crust. The molten Al can now penetrate outside through the pores and cracks and is immediately oxidized when getting in contact with air. Therefore, the needles and plate on the surface of particle can be shown in Fig. 8.

Figure 9a and b, depicts the product obtained from TG–DTA experiment, at the maximum temperature of 1,400 °C using the heating rate of 20 °C/min. Therefore, as it is observed in Fig. 9a, b, if the temperature is increased (in region IV) so high that the applied force on the crust can overcome the strength of the crust, then the

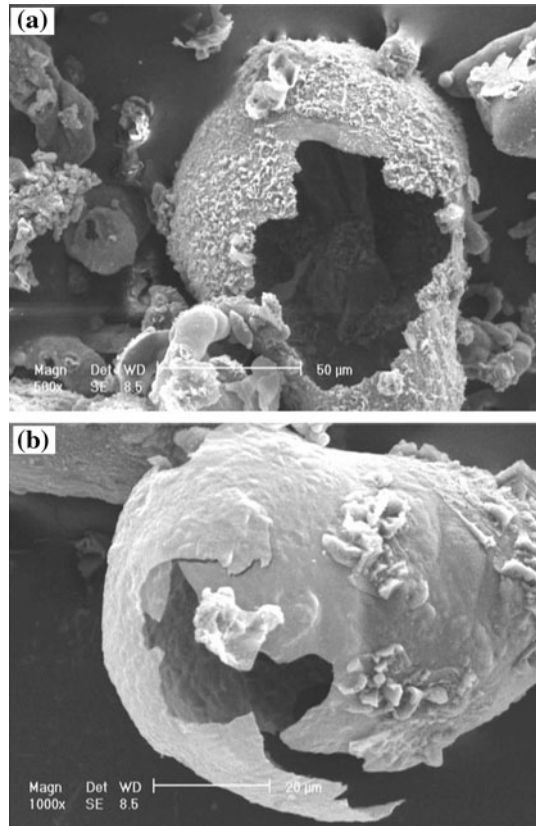
Fig. 9 SEM micrographs of aluminum particles after being oxidized at the maximum temperature of 1,400 °C by the heating rate of 20 °C/min; **a** the permeation of melted aluminum to the outside of the oxide crust (especially at grain boundaries) and its oxidation immediately after exiting the crust and **b** the burst of an aluminum particle and the remaining part of the torn oxide crust



crust is broken and the melt will permeates out. As a result, the rate of oxidation is suddenly and intensively increased. Microscopic studies performed on the morphology of the products of these samples, tear of the crust, diffusion of the melt, and intense oxidation resulting from it, are well substantiated according to these images. Because of the weak and low strength of the grain boundary, it is expected that the crack of the crusts starts from the grain boundary at the initial stages. This phenomenon is observable in the microscopic image presented in Fig. 9a. Additionally, according to Fig. 9b, it can be determined that the thickness of the oxide layer in this state is about 1 μm .

Since the rate of the melt expansion inside the oxide crust is greatly dependent on the volume of the melt remaining inside the particle and the heating rate (as mentioned in “[Thermal Analysis](#)” section), therefore the size of the particles, the thickness of the initial amorphous oxide crust, and the particles heating rate can greatly affect it. To study it more precisely, an amount of aluminum powder at isothermal conditions was heated at 900 °C for 15 min. The SEM images taken from the place of the burst of the oxide crusts are well observed in Fig. 10a, b. As it is observed in these samples, by increasing the heating rate of aluminum particles (at isothermal conditions), the melt was able to tear the oxide crust at a lower temperature relative to the samples under non-isothermal conditions. That is

Fig. 10 SEM micrographs of the burst of the aluminum particles and the remaining part of the torn oxide crusts (isothermally heat treated at 900 °C for 15 min), by various magnifications



because of the lower strength of the oxide crust and the added heat tension in these conditions. For this reason, an intense thermal shock is exerted on the Al_2O_3 ceramic crust when the samples are placed in the furnace at isothermal conditions; therefore, under the influence of this factor, the tear of the oxide crust takes place at a lower temperature.

Phase Analysis

The X-ray diffraction pattern of the aluminum particles at the ambient temperature and that of the aluminum powders oxidized as non-isothermal by TG-DTA experiment at the maximum temperatures of 720, 900 and 1,400 °C at the heating rate of 20 °C/min are depicted in Fig. 11a–d, respectively. In Fig. 11a, b, the crystalline aluminum without a trace of the aluminum oxide is observed. While, according to Fig. 6a, b, the amorphous oxide layer is changed into alumina with crystalline structure at 720 °C (according to Fig 1). In fact, it can be reasoned that this is done due to a little amount of the aluminum oxide in the sample. But, as it is observed in Fig. 11c, d, by increasing the temperature from 900 to 1,400 °C, the X-ray diffraction patterns of these samples confirm the presence of a great amount of aluminum residual with a small amount of $\alpha\text{-Al}_2\text{O}_3$ phase among the products.

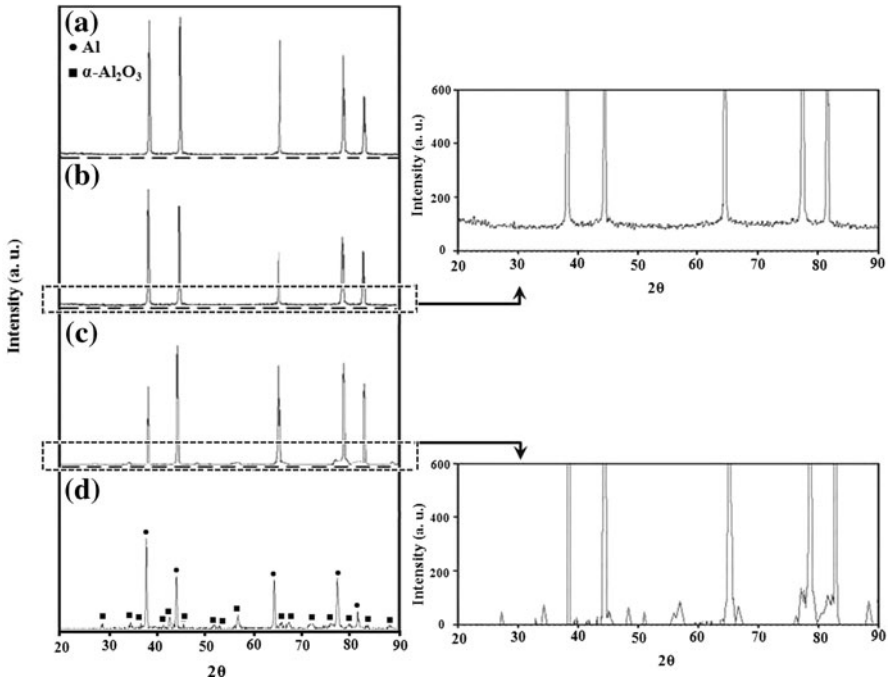


Fig. 11 XRD patterns of the aluminum particles **a** before experiment, and after being oxidized at the maximum temperature of **b** 720, **c** 900 and **d** 1,400 °C by the heating rate of 20 °C/min

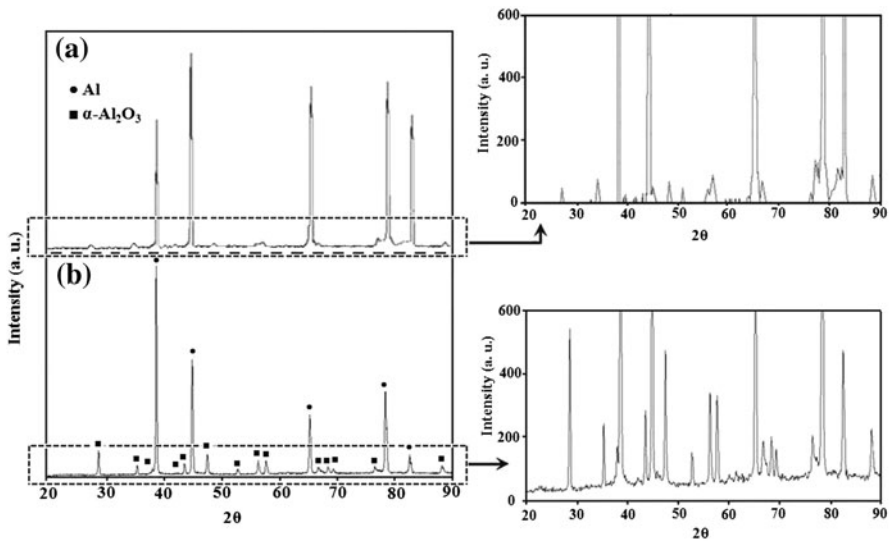


Fig. 12 XRD patterns of the aluminum particles after being oxidized; **a** at the maximum temperature of 900 °C by the heating rate of 20 °C/min, and **b** at 900 °C for 15 min (under isothermal conditions)

Then, it can be concluded that only a part of the particle oxidation is taken place and the major part remains non-reacted. Another point well inferred from Fig. 11 is that, the γ - Al_2O_3 phase is changed into α - Al_2O_3 phase up to 900 °C.

The products of the two oxidized samples under non-isothermal (heating rate: 20 °C/min and T_{max} : 900 °C) and isothermal (heated at 900 °C for 15 min) conditions were analyzed through XRD (Fig. 12a, b, respectively) to study the effect of the particles heating rate on the aluminum oxidation process. By comparing the X-ray diffraction patterns of the two samples in Fig. 12a, b, it is observed that the diffraction peak intensity of α - Al_2O_3 phase becomes more intense as heating rate increases. This means that the rate of oxidation of aluminum powder particles is greatly dependent on the heating rate which can be confirmed by the microstructure observations (Figs. 7, 10) and intense peaks in the RTG curves (Fig. 2).

Conclusions

The following conclusions can be drawn from this study on the mechanism of the oxidation process of pure aluminum powder particles within the temperature range of 25–1,400 °C.

The oxidation of aluminum powders occurred at different stages. In the initial stage, the rate of oxidation was very negligible; wherein the amorphous oxidation crust properly protected aluminum up to this limit. In continuation, the amorphous oxide crust was changed into crystalline phase by increasing the temperature up to the limit of 600 °C. Because of the formation of grain boundary in the structure of the crust through crystallization, the oxidation rate is increased. But, by increasing the temperature up to 700 °C, the diffusion paths were destroyed by the effect of oxidation process so that the rate of oxidation was abruptly reduced. So, there was no noticeable sign of mass gain increase resulting from oxidation. Also, during this stage, the remaining aluminum present in the particles was melted. In continuation, the melt within the crust was expanded by an increase in temperature. Also in this stage, the shrinkage of crust occurred during γ - Al_2O_3 to α - Al_2O_3 transformation. Due to this expansion of molten aluminum and shrinkage of crust, it created an intense tension on the crust. Within the temperature range of 1,000–1,150 °C, the melt ruptured the crust and permeated outward. The contact of this melt with oxide atmosphere made an intense oxidation. The main stage of the oxidation of aluminum powder particles was oxidized at this stage.

Therefore, considering the temperature at all stages, it can be concluded that the mechanism of oxidation on the surface of aluminum particles was the controlled diffusion. On the other hand, it can also be concluded that the complete oxidation of aluminum particles did not take place even up to 1,400 °C. But, it should be added that the total value of oxidation can be changed by the heating rate.

References

1. E. W. Price, and R. K. Sigman, in *Combustion of Aluminized Solid Propellants*, eds. V. Yang, T. Brill, and W. Ren, (American Institute of Aeronautics and Astronautics, 2000), p. 663.

2. H. Dong and S. Zhumei, *Combustion and Flame* **105**, (3), 428 (1996).
3. S. Wang, K. Liang, X. Zhang, H. Li and S. Gu, *Key Engineering Materials* **224–226**, 745 (2002).
4. L. Galfetti, L. T. DeLuca, F. Severini, G. Colombo, L. Meda and G. Marra, *Aerospace Science and Technology* **11**, 26 (2007).
5. F. Maggi, A. Bandera, L. Galfetti, L. T. De Luca and T. L. Jackson, *Acta Astronautica* **66**, 1563 (2010).
6. L. Galfetti, L. T. De Luca, F. Severini, L. Meda, G. Marra, M. Marchetti, M. Regi and S. Bellucci, *Journal of Physics: Condensed Matter* **18**, S1991 (2006).
7. L. T. De Luca, L. Galfetti, F. Severini, L. Meda, G. Marra, A. B. Vorozhtsov, V. S. Sedoi and V. A. Babuk, *Combustion, Explosion, and Shock Waves* **41**, (6), 680 (2005).
8. M. A. Trunov, M. Schoenitz and E. L. Dreizin, *Propellants, Explosive, Pyrotechnics* **30**, 1 (2005).
9. A. G. Alekseev, R. A. Barlas, T. I. Tsidelko, and A. F. Shapoval, in *Effect of Particle Size on the Combustibility and Explosion Parameters of Dispersed Aluminum and Magnesium Powders*, ed. V. V. Nedin, (Preduprezhdenie Vnezapnykh Vzryvov Gazodispersnykh Sistem, 1971), p. 66 (in Russian).
10. A. F. Belyaev, Y. V. Frolov and A. I. Korotkov, *Fiz Goreniia Vzryva* **4**, (3), 323 (1968) (in Russian).
11. C. Brossard, A. Ulas, C. L. Yen, and K. K. Kuo, in *16th International Colloquium on the Dynamic of Explosions and Reactive Systems*, Krakow, Poland, 3th–8th August (1997).
12. M. E. Derevyga, L. N. Stesik and E. A. Fedorin, *Combustion, Explosion, Shock* **13**, (6), 722 (1977).
13. V. A. Ermakov, A. A. Razdobreev, A. I. Skorik, V. V. Pozdeev and S. S. Smolyakov, *Fiz Goreniia Vzryva* **18**, (2), 141 (1982) (in Russian).
14. C. Johnson, T. Parr, D. Hanson-Parr, R. Hollins, S. Fallis, and K. Higa, *Proceedings 37th JANNAF Combustion Subcommittee Meeting*, 13th–17th November, (2000), p. 539.
15. V. I. Rozenband and N. I. Vaganova, *Combustion and Flame* **88**, (1), 113 (1992).
16. Y. Zhu and S. Yuasa, *Combustion and Flame* **115**, 327 (1998).
17. L. P. H. Jeurgens, W. G. Sloof, F. D. Tichelaar and E. J. Mittemeijer, *Physical Review B* **62**, 4707 (2000).
18. L. P. H. Jeurgens, W. G. Sloof, F. D. Tichelaar and E. J. Mittemeijer, *Thin Solid Films* **418**, 89 (2002).
19. L. P. H. Jeurgens, W. G. Sloof, F. D. Tichelaar and E. J. Mittemeijer, *Surface Science* **506**, 313 (2002).
20. L. P. H. Jeurgens, W. G. Sloof, F. D. Tichelaar and E. J. Mittemeijer, *Journal of Applied Physics* **92**, (3), 1649 (2002).
21. V. Kolarik, M. M. Juez-Lorenzo and H. Fietzek, *Materials Science Forum* **696**, 290 (2011).
22. J. C. Sanchez-Lopez, A. R. Gonzalez-Elipse and A. Fernandez, *Journal of Materials Research* **13**, 703 (1998).
23. O. A. Riano, J. Wadsworth and O. D. Sherby, *Acta Materialia* **51**, 3617 (2003).
24. M. A. Trunov, M. Schoenitz, X. Zhu and E. L. Dreizin, *Combustion and Flame* **140**, 310 (2005).
25. N. Eisenreich, H. Fietzek, M. M. Juez-Lorenzo, V. Kolarik, A. Koleczko and V. Weiser, *Propellants, Explosives, Pyrotechnics* **29**, 3 (2004).
26. V. Weiser, S. Kelzenberg and N. Eisenreich, *Propellants, Explosives, Pyrotechnics* **26**, 284 (2001).
27. I. Levin and D. Brandon, *Journal of American Ceramic Society* **81**, 1995 (1998).